Carbohydrate Polymers 340 (2024) 122299

Contents lists available at ScienceDirect

Carbohydrate Polymers

journal homepage: www.elsevier.com/locate/carbpol

Alternative proton exchange membrane based on a bicomponent anionic nanocellulose system

Fernanda Brito dos Santos [a,b], Joice Kaschuk [a,c,d], Gabriel Banvillet [b], Adel Jalaee [a], Orlando J. Rojas [a,b,c], E. Johan Foster [a,b,*]

[a] Department of Chemical and Biological Engineering, The University of British Columbia, Vancouver, BC, Canada, V6T 1Z3
[b] Bioproducts Institute, University of British Columbia, 2360 E Mall, Vancouver, BC V6T 1Z3, Canada
[c] Department of Bioproducts and Biosystems, Aalto University, Espoo, Finland
[d] Physical Chemistry and Soft Matter, Wageningen University & Research, 6708, WE, Wageningen, Netherlands

ARTICLE INFO

Keywords:
TEMPO-oxidized CNF
Sulfonated CNF
Ion exchange membranes
Fuel cells
Nanocellulose

ABSTRACT

As integral parts of fuel cells, polymer electrolyte membranes (PEM) facilitate the conversion of hydrogen's chemical energy into electricity and water. Unfortunately, commercial PEMs are associated with high costs, limited durability, variable electrochemical performance and are based on perfluorinated polymers that persist in the environment. Nanocellulose-based PEMs have emerged as alternative options given their renewability, thermal and mechanical stability, low-cost, and hydrophilicity. These PEMs take advantage of the anionic nature of most nanocelluloses, as well as their facile modification with conductive functional groups, for instance, to endow ionic and electron conductivity. Herein, we incorporated for the first time two nanocellulose types, TEMPO-oxidized and sulfonated, to produce a fully bio-based PEM and studied their contribution separately and when mixed in a PEM matrix. Sulfonated nanocellulose-based PEMs are shown to perform similarly to commercial and bio-based membranes, demonstrating good thermal-oxidative stability (up to 190 °C), mechanical robustness (Young's modulus as high as 1.15 GPa and storage moduli >13 GPa), and high moisture-uptake capacity (ca. 6330 % after 48 h). The introduced nanocellulose membranes are shown as promising materials for proton-exchange material applications, as required in fuel cells.

1. Introduction

Renewable energy is a key component to the global decarbonization strategy, which requires green alternatives to conventional energy sources along with progress in governmental regulations and technological advances (Kim & Yang, 2023). In this context, electrochemical cells are critical enabling technologies for energy management, conservation, and storage, as well as pollution control/monitoring and greenhouse gas reduction (Badwal, Giddey, Munnings, Bhatt, & Hollenkamp, 2014; García, Torrero, Retuerto, & Rojas, 2022; Irannejad & Rezaei, 2022; Winter & Brodd, 2004).

Many electrochemical energy technologies have been developed in the past year, and fuel cells (FCs) serve as an example of this. Among different types of FCs, polymer electrolyte membrane fuel cells (PEMFCs) stand out as the most common and efficient electrochemical cells (Abaspour, Tadrisi Parsa, & Sadeghi, 2014; Wang, Swihart, & Wu, 2019). This FC type utilizes a PEM as part of its cell stack, which consists of a semipermeable membrane designed to transport cations, separate reactant gases, and work as an electronic insulator (Baker & Zhang, 2011). Currently, the most common PEMs are made of sulfonated polytetrafluoro-ethylene (Nafion). The targeted ionic properties and hydrophilicity are obtained with sulfonic acid groups combined with electronegative fluorine atoms ($–CF_2$, $–SO_3H$), while the bulk polymer matrix, a tetrafluoroethylene (PTFE) backbone, is hydrophobic and confers mechanical and thermal stability to the membrane (Feng et al., 2015; Peighambardoust, Rowshanzamir, & Amjadi, 2010). Although Nafion has superior performance compared to other commercial low temperature PEMs, this material is limited by factors including high cost, insufficient durability and limited power density. When disposed of, Nafion is a potential source of numerous perfluorinated compounds, including toxic perfluorocarboxylic acids (PFCAs) and others that are environmentally persistent and bioaccumulative. These chemicals are widespread across the globe and are found at concentrations of ng/mL in human blood and associated with tumor growth, developmental and

* Corresponding author.
E-mail address: johan.foster@ubc.ca (E.J. Foster).

https://doi.org/10.1016/j.carbpol.2024.122299
Received 21 January 2024; Received in revised form 17 May 2024; Accepted 19 May 2024
Available online 20 May 2024

hormonal issues, and immunotoxicity (Di Virgilio et al., 2023; Feng et al., 2015; Peighambardoust et al., 2010; Zhu et al., 2022).

Cellulose and modified cellulose have been considering for both electrodes and ion-exchange membranes. They benefit from high wettability, good mechanical properties, thermal stability, and controllable porosity and thickness, which are all essential properties for ion-exchange membranes (IEMs) (Jalaee, Kamkar, French, Rojas, & Foster, 2023; Vilela, Silvestre, Figueiredo, & Freire, 2019). Several researcher groups have highlighted the potential of both cellulose nanocrystals (CNC) and cellulose nanofibers (CNF) for application in energy devices due to their physical, mechanical, thermal, chemical, and optical stability as well as their gas-barrier properties. Applying pure cellulose as an IEM, Bayer et al. (2016) and Gadim et al. (2014) showed high H_2 barrier properties. They reported a CNC membrane of 30 mm thickness, 65 % crystallinity and 0.018 cm^3/g total mesoporous volume presenting a H_2 permeability of 0.01 barrer, and maximum proton conductivity and power density of 4.6 mS/cm (at 120 °C, 100%RH) and 17.2 mW/cm^2 (at 80 °C, 95%RH), respectively. In the case of CNF membranes of 32 mm thickness, 51 % crystallinity and 0.016 cm^3/g total mesoporous volume, a H_2 permeability of 0.02 barrer and maximum proton conductivity and power density of 0.05 mS cm^{-1} (at 100 °C, 100%RH) and 0.79 mW/cm^2 (at 80 °C, 95%RH), were demonstrated. These results clearly show CNC and CNF with permeability values three orders of magnitude lower than those of Nafion ($< 10^{-1}$ barrer for Nafion).

Cellulose itself has no electrochemical activity (proton/cation transport) when applied in fuel cells. This can be changed through modifications of cellulose with negative functional groups, which have been shown to be a promising approach. For instance, in dry conditions, better proton conductivity can be obtained by using CNCs carrying sulfonic acid groups (Bayer et al., 2016). However, this behavior was not verified for carboxylated cellulose (TEMPO nanocellulose), given the proportional relationship between humidity and conductivity (Guccini et al., 2019).

The effect of cellulose in polymer matrix structures has been studied in the literature. A representative example in this domain includes the work of Hou et al. (2017) regarding membranes of sulfonated poly(aryl ether ketone) (SPAEK) containing sulfonic and carboxylic groups and reinforced with CNCs (2, 5, 8 and 10 wt%). A membrane composed of SPAEK with 10 % carboxylic group content and 5 wt% CNC presented a Young's modulus (ca. 526 MPa, wet) that is 1.5 times higher than the pure SPAEK matrix (ca. 350 MPa). Moreover, this membrane with a water-uptake ability of ca. 77 % (at 80 °C) and an IEC of 2.49 meq/g exhibited a protonic conductivity of 272 mS/cm at 80 °C, which is 1.7 times higher than that of the pure SPAEK membrane (163 mS/cm).

Cai et al. (2018) embedded phosphoric acid-doped (0.25 mol/cm^3) CNF into a sulfonated-SPES matrix (95 wt%). The membranes with a thickness of 85–120 mm presented a tensile strength of 28 MPa, water uptake capacity of 43 % (at 80 °C), IEC of 1.52 mmol/g and proton conductivity of 154 mS/cm at 80 °C and 100 % RH. Similarly, Xu et al. (2018) prepared membranes based on SPES and CNF (5 wt%) with a tensile strength of 40 MPa, water-uptake capacity of 40 % at 80 °C, and proton conductivity of 130 mS/cm at 80 °C and 100%RH. The hydrophilicity of the PEMs increased with the increasing CNF content from 1 to 5 wt%.

In this research, we combined TEMPO-oxidized and sulfonated nanocellulose as a bio-based PEM. The effect of both COO^- groups (from TEMPO-oxidized CNF) and SO_3^- groups (from sulfonated CNF) on the electrochemical properties was assessed. We hypothesized that the combination of these ionic groups is effective in altering the membrane's conductivity by enhancing the transport of H^+ ions. This is the first study to investigate the impact of both conductive groups separately and in tandem, with the goal of determining the optimal composition for a bio-based PEM made from modified cellulose. In this study, we propose a component that can fully or partially replace the current PFCA compounds found in commercial PEMs. Moreover, we evaluated the thermal stability, mechanical and morphological properties, chemical structure, water uptake, ion exchange capacity (IEC) and proton conductivity of the biobased membranes and evaluated their performance as a bio-based PEM in a fuel cell application.

2. Experimental section

2.1. Materials

Bleached eucalyptus kraft pulp was purchased from Fibria, Brazil (dry pulp sheets, molecular weight of 162 g/mol, cellulose content of 90 %, xylan content of 9.5 %, and lignin content of 0.5 %). Chemicals were used as received from suppliers: sodium hydroxide (NaOH ≥97.0 %, Sigma-Aldrich), sodium hypochlorite (NaClO 10–15 %, Sigma-Aldrich), sodium bromide (NaBr ≥99.0 %, Sigma-Aldrich), sodium bisulfite ($NaHSO_3$ ≥ 58.5–67.4 %, Thermo Fisher Scientific), hydrochloric acid (HCl 37 %, Sigma-Aldrich), TEMPO (2,2,6,6-tetrametylpiperidine-1-oxyl, $C_9H_{18}NO$, 98 %, Sigma-Aldrich), sodium periodate ($NaIO_4$ ≥ 99.8 %, Sigma-Aldrich), isopropanol ($(CH_3)_2CHOH$ ≥ 99.5 %, Sigma-Aldrich).

2.2. Membrane preparation

2.2.1. Precursor fiber processing

Cellulose fibers were first refined with a laboratory PFI mill to increase cellulose accessibility. After dispersion at a solid content of 10 wt %, the pulp was refined for 10,000 revolutions, until reaching a value of 100 CS (68 SR) as measured with a Canadian Standard Freeness Tester following the ISO 5267-2 standard. The pulp was then diluted to 1 wt% for further modification.

Sulfonation was performed on 10 g of refined pulp (dry equivalent) with two steps: (i) anhydroglucose unit (AGU) ring opening by periodate oxidation, using a sodium periodate ratio of 1.350 g/g of cellulose (Liimatainen, Visanko, Sirviö, Hormi, & Niinimäki, 2013), and (ii) aldehyde conversion into sulfonate groups, using a sodium bisulfite ratio of 1.284 g/g of cellulose, i.e. 12.34 mmol/g of cellulose, the maximal aldehyde content if the periodate oxidation was complete. The periodate oxidation was carried out under constant stirring for 30 h at 30 °C, with a solid content of 0.5 wt%. During this step, cellulose depolymerization by side reactions was prevented by covering the glassware with aluminum foil to avoid light, and by using 6.3 vol% of isopropanol in the reaction, acting as a radical scavenger (Larsson, Kochumalayil, & Wågberg, 2013; Painter, 1988). The pulp was then extensively washed with deionized water until the filtrate displayed a conductivity below 5 μS/cm, and a sample was retrieved for titration and FTIR spectroscopy. The sulfonation was then carried out under constant stirring for 72 h at room temperature, with a solid content of 0.5 wt%. The sodium bisulfite amount (12.34 mmol/g) represented 3.9 times excess with respect to the aldehyde content, which was measured to be 3.13 mmol/g.

TEMPO-mediated oxidation was performed on 10 g of refined pulp (dry equivalent) with TEMPO/NaBr/NaClO ratios of 0.1 mmol/1 mmol/5 mmol per gram of cellulose, respectively (Saito, Kimura, Nishiyama, & Isogai, 2007). The reaction was carried out under constant stirring at 25 °C, with a solid content of 1 wt%. TEMPO and NaBr were first dissolved in purified water and mixed with the pulp for 5 min. After adding NaClO, a stable pH of 10.0 ± 0.1 was maintained by adding 3 M NaOH dropwise, until pH stabilized. The reaction was then quenched by lowering the pH to 7 with 3 M HCl.

After both reactions, the modified fibers were extensively washed with deionized water until the filtrate displayed a conductivity below 5 μS/cm. A 1-μm nylon sieve (Sefar, Switzerland) was used to prevent fiber loss during filtration.

2.2.2. Fibrillated cellulose (T-CNF and S-CNF)

The modified fibers were fibrillated into CNF using a M-110P microfluidizer (Microfluidics, USA) equipped with an 87-μm Z-type

chamber. The TEMPO-oxidized fibers were diluted to 0.87 wt% and the pH was set to 8.20 with 3 M NaOH, before processing for 2 passes at 1800 bar and 2000 bar, in sequence. The sulfonated fibers were diluted to 0.63 wt% and the pH was set to 8.0 with 3 M NaOH, before processing it for 5 passes with a gradually increasing pressure from 1700 bar to 2000 bar. A greater number of passes was used for the sulfonated pulp, which could be processed with a higher flow than the TEMPO-oxidized pulp, due to its lower viscosity. This enabled a comparable residence time in the process for both samples.

2.2.3. T-CNF and S-CNF morphology

Sample preparation was carried out with a 10^{-3} wt% dilute CNF suspension, homogenized for 2 min with an Ultra-Turrax T-25 disperser (IKA, Germany) working at 8000 rpm. A drop of the suspension was deposited on a freshly cleaved mica plate and allowed to dry at room temperature. The sample was then imaged using a Jupiter XR Atomic Force Microscope in tapping mode, equipped with a 10 nm tip radius FS-1500 Silicon probe (Oxford Instruments, 1500 kHz resonance frequency, 6 N/m spring constant). Typically, images of 5 × 5 μm and 2 × 2 μm were acquired with a resolution of 1024 points per line, and treated using the Gwyddion software, for levelling (mean plane subtraction), horizonal scars correction, and height adjustment. An analysis of 100 randomly selected CNFs was made to assess their height and length distribution.

2.2.4. T-CNF and S-CNF charge and chemical features

For T-CNF and S-CNF titration, 20 mg of CNF (dry equivalent) were diluted in 500 mL of 1 mM NaCl and stirred for 1 h to ensure a complete and homogeneous dispersion. 3 mL of 0.01 M HCl were then added, and the suspension was stirred for an additional hour. The titration was then carried out dropwise with 0.01 M NaOH, to determine the carboxylic acid and sulfonic acid contents in mmol/g of cellulose for T-CNF and S-CNF, respectively. The conductivity was constantly corrected to account for the added NaOH volume.

Zeta potential was measured with Zetasizer Nano ZS-90 (Malvern) to assess the surface charge density of the T-CNF and S-CNF samples using the dip-cell system. The suspension concentrations were all equal to 0.01 g/L and their pH was adjusted by adding controlled volumes of 0.1 M NaOH and 0.1 M HCl solutions. Analysis and discussion of zeta potential results can be found in the Supplementary Information.

FTIR analysis was used to identify the modification of the cellulose fibers before and after the oxidation reactions. The CNF suspensions were analyzed separately with an IR spectrophotometer Spectrum 100 (Bruker, DE), with attenuated total reflectance (ATR) attachment. Samples were measured at a spectral range of 4000-600 cm^{-1}, with 32 scans, and a resolution of 4 cm^{-1}.

Powder samples were obtained by freeze drying 0.1 wt% CNF suspensions. The resulting coarse powders were then gently crushed with a mortar and pestle, to avoid any degradation of the cellulose crystalline structure. 13C CP-MAS NMR spectra, with high power proton decoupling, were collected on a 400 MHz Bruker solid state wide bore AVANCE spectrometer. Samples were spun at 6 kHz at magic angle. 13C pulse with a ramped amplitude at 50 % was used for cross polarization with a contact time of 5 ms. Relaxation delay and acquisition time were set to 5 s and 50 ms respectively. Data was processed with 50 Hz line broadening exponential decay function prior to Fourier Transform. Chemical shift values (ppm) were referenced with adamantane prior to data acquisition. All experiments were done at room temperature.

2.2.5. Membrane fabrication

The various membranes were prepared by filtration and hot pressing using a previously outlined procedure (Banvillet, Depres, Belgacem, & Bras, 2021). The CNF suspension was diluted to 0.5 wt% and degassed under vacuum for 2 h to remove all bubbles in the suspension. Homogenization ensured a complete mixing of both CNF types together, using an Ultra-Turrax T-25 disperser (IKA, Germany) at 8000 rpm for 10 min. The suspension was then filtered with a 142 mm Büchner funnel equipped with a 0.22 μm PVDF membrane (Merck, Germany), until the CNF mat exhibited a semi-dry aspect (solid content of approx. 15 wt%). *The following step used decompression filtration (Vacuubrand, Model: MD 4C NT + AK + EK at 1.5 mbar) to prepare all CNF modified membranes*. The CNF mat was placed between the PVDF membrane on one side and a 1 μm nylon sieve (Sefar, Switzerland) on the other side, while blotting papers were added above it. This stack was then dried by hot pressing at 70 °C and 0.1 bar for 1 h, until complete removal of water from the CNF mat. The resulting dry membranes were stored in a conditioned room at 23 °C and 50 %RH for 48 h before beginning characterization.

The membrane thickness is an important determinate when considering proton exchange membrane efficiency (Baker & Zhang, 2011). Therefore, this parameter was kept constant for each membrane, independent of its composition in both CNF types. The amounts of CNF used (dry equivalent) therefore varied for each membrane and are summarized in Table 1 below.

2.3. Modified CNF membrane properties

2.3.1. Membrane morphology

The cross-sectional images of the membranes were analyzed using Scanning Electron Microscopy (SEM) (Helios NanoLab 650, FEI, Hillsboro, OR, USA) operated at an acceleration voltage of 1.0 kV. Accordingly, the cross-section of the samples was cut *by employing the ultramicrotomy method using a diamond knife*, placed on top of SEM holders vertically, and coated with 6 nm layer of Iridium (Ir) using a Cressington sputter.

2.3.2. Structural properties

The crystallinity of the samples was determined by X-ray diffraction spectroscopy. XRD patterns of the CNF modified membranes were acquired by using a Malvern Panalytical, Empyrean 3 instrument at CuKα radiation (λ = 0.15406 nm). The CuKα radiation was generated from Cu anode supplied with 45 kV and a current of 40 mA over a range of 2θ value from 5 to 90° with the scan step size of 0.025° at a scanning speed of 2°/min. Crystallinity was defined as the ratio between the area of the crystalline peaks and the total area of peaks, as reported in Eq. (1).

$$Crystallinity\ (\%) = \frac{Area\ of\ the\ crystalline\ peaks}{Total\ area\ of\ peaks} \times 100 \quad (1)$$

2.3.3. Thermal properties

Thermogravimetric curves were obtained for all modified CNF membranes (100:0, 75:25, 50:50, 25:75, and 0:100) to evaluate the temperature range that these membranes can operate before their degradation starts. All samples were heated to 800 °C at 10C°/min, with a nitrogen flow rate of 20 cm^3/min.

2.3.4. Mechanical properties

Dynamic Mechanical Analysis (DMA) was performed on a TA Q850. The membranes were cut in rectangular shapes into 0.5 cm × 2 cm. The

Table 1
Composition and properties of each membrane. CNF amounts (g) are the dry equivalent masses used at the beginning of the membrane formation process. Grammage and thickness are measured after 48 h of storage in the conditioned room (23 °C, 50 %RH).

T-CNF/S-CNF ratio	[a]T-CNF (g)	[a]S-CNF (g)	Grammage (g. m^{-2})	Thickness (μm)
100:0	1.08	0	56.9	46.2
75:25	0.93	0.31	67.2	48.7
50:50	0.70	0.70	68.1	50.0
25:75	*0.39*	1.16	69.6	50.7
0:100	0	1.70	72.3	48.9

[a] T-CNF: TEMPO-oxidized CNF; S-CNF: Sulfonated CNF.

tests were carried out with a frequency of 1 Hz, 1 N applied pre-force, and an oscillation amplitude of 10 μm. The storage modulus (E') and tan delta were obtained at a heating rate of 3 °C/min in air with a temperature range from 20 to 200 °C, and in an oscillatory tensile mode with humidity control. Throughout the experiment, relative humidity was held constant at 90 %. The temperature was raised from 30 to 90 °C.

Tensile measurements (TA Instrument, DMTA-850) were run at $20\,\mu m.\,min^{-1}$ with an extension rate in displacement ramp control from the inherited elongation to 200 μm. To this end, membrane films, which were cut into rectangular shapes into 0.5 × 2 cm, were tested at two constant temperatures of 25 °C and 80 °C and at room and 98 % RH.

2.3.5. Water uptake and degree of swelling

The hydrophilic properties of all membranes were studied by measuring their water uptake in DI water at 25, 40, 60, and 80 °C following ASTM D570 (D20 Committee, n.d). In this method, a dry sample was weighted (m_0), immersed in water for 48 h, and weighted again to obtain the maximum mass gain (m_{max}) of the samples. The water uptake was defined as the ratio between the absorbed water and the mass of the dried membrane as reported in Eq. (2).

$$\%Water\ uptake\ (WU) = \frac{m_{max} - m_0}{m_0} \times 100 \quad (2)$$

2.3.6. Oxidative test

Following procedures based on prior literature (Bayer et al., 2021; Zhao et al., 2019), the chemical stability of modified CNF membranes was investigated by using Fenton's test. The samples were vacuum dried at 80 °C for two hours, and then their dry weight was measured. The samples were then immersed into Fenton's reagent (3 ppm $FeSO_4$ in 3 % H_2O_2) at 80 °C for one hour. Finally, the samples were vacuum dried again and their weight loss was determined. The residual weight (RW) % was calculated from the difference between the weight of the samples before (m_0) and after treatment (m_f) using Eq. (3).

$$RW(\%) = \frac{m_f}{m_0} \times 100 \quad (3)$$

2.3.7. Ion Exchange Capacity (IEC)

The IEC values of the prepared membranes were determined by potentiometric titration. The dried membrane samples were weighed, and then immersed in NaCl solution 1 M for 24 h to liberate H^+ ions. The exchanged protons within the solutions were then titrated with 0.1 M NaOH aqueous solution to pH 7. IEC values were calculated using the following Eq. (4):

$$IEC = \frac{C_{NaOH} \times V_{NaOH}}{W_{dry}} \quad (4)$$

where C_{NaOH} and V_{NaOH} are the concentration and volume of titrated NaOH solution and W_{dry} is the weight of the dry membrane.

2.3.8. Hydration number

Hydration number, λ, defined by the number of water molecules associated per sulfonic acid group in the proton exchange membrane was also calculated for the water uptake and IEC using the following Eq. (5) (Sharma & Kim, 2022).

$$\lambda = \frac{10 \times WU}{IEC \times 18.02} \quad (5)$$

2.3.9. Proton conductivity

The through-plane proton conductivity of all membranes was determined by AC Electrochemical Impedance Spectroscopy (EIS) (Solartron SI 1260) by using a frequency response analyzer with a frequency range of 1000 to 1×10^7 kHz with an amplitude of 0.1 mV at room temperature. Before performing the measurement, the membranes were fully hydrated for 24 h. Proton conductivity was calculated from the following Eq. (6), where R is the resistance, L is the thickness, and S is the area of the tablet.

$$\sigma = \frac{L}{RS} \quad (6)$$

3. Results and discussion

3.1. Modified CNF suspensions

3.1.1. CNF modification and characterization

Herein, cellulose nanofibrils bearing sulfonate (SO_3^-) and carboxylate groups (COO^-) were obtained from sulfonation and TEMPO-oxidation routes, respectively. Both approaches target different carbons in the anhydroglucose unit (AGU), and therefore result in distinct cellulose structures, as shown in Fig. 1a.

The sulfonation route requires an intermediate step of periodate oxidation, which converts the two *secondary alcohols* of the AGU into aldehydes, resulting in 2,3-dialdehyde cellulose (DAC) (Plappert et al., 2018), which involves a disruption of the C2-C3 covalent bond, in the ring-opening. The efficiency of this reaction was assessed by FTIR spectroscopy (Fig. 1b) and its discussion can be found in the supporting information (SI).

3.1.2. Morphology

Statistical analyses were performed on AFM images of the CNF samples, to provide quantitative information about their respective morphologies (Fig. S1). All values display log-normal distributions, in accordance with previous work (Mattos, Tardy, & Rojas, 2019).

Sulfonation and TEMPO-oxidation routes lead to well-individualized nanoscale elements, with average widths of 3.29 ± 2.09 nm and 2.60 ± 0.68 nm, respectively. These values indicate that both routes result in cellulose elementary fibrils, the smallest native cellulose chains conformation (Kubicki et al., 2018; Thomas et al., 2012). The shorter CNF lengths of 329 ± 213 nm (S-CNF) and 273 ± 142 nm (T-CNF) can be attributed to their respective high charge contents of 0.47 mmol/g and 2.39 mmol/g, respectively. (Benhamou, Dufresne, Magnin, Mortha, & Kaddami, 2014). The 1700–2000 bar pressure during homogenization may have also caused this length decrease (Spence, Venditti, Rojas, Habibi, & Pawlak, 2011; Taheri & Samyn, 2016). A deep discussion on the AFM results as well as the zeta potential results can be also found in the SI for all analyzed samples.

3.2. Membranes characterizations

3.2.1. Structure of the modified CNF membranes

SEM images of membrane cross-sections were then taken to determine whether possible rupture and void spaces exist within the modified CNF membranes (Fig. 2a –2e).

As observed in Fig. 2a–e, all samples exhibit compactness and homogeneity throughout the membrane cross-sections. This is due to the ability of the highly surface-modified short fibrils to pack closely into dense homogeneous layers rather than interacting to form fibril bundles during the film formation process. The layered structure of these types of nanofibers have been detected before and attributed to the process of fibril dewatering; the resulting anisotropy of the membrane also favors unidirectional swelling. The density of these membranes contributes to the absence of void spaces and ruptures, demonstrating that these films can effectively block crossover of H_2 and O_2, improving fuel cell efficiency and reducing potential for dangerous degradation hotspots in the fuel cell (Lander et al., 2022).

3.2.2. Chemical structure, thermal, and mechanical stability

FTIR analysis of the modified CNF membranes (Fig. 3a) reveals relatively equivalent spectra to the results presented in Fig. 1b, with lower intensities around 3300 cm^{-1} (O—H stretching) mainly due to the

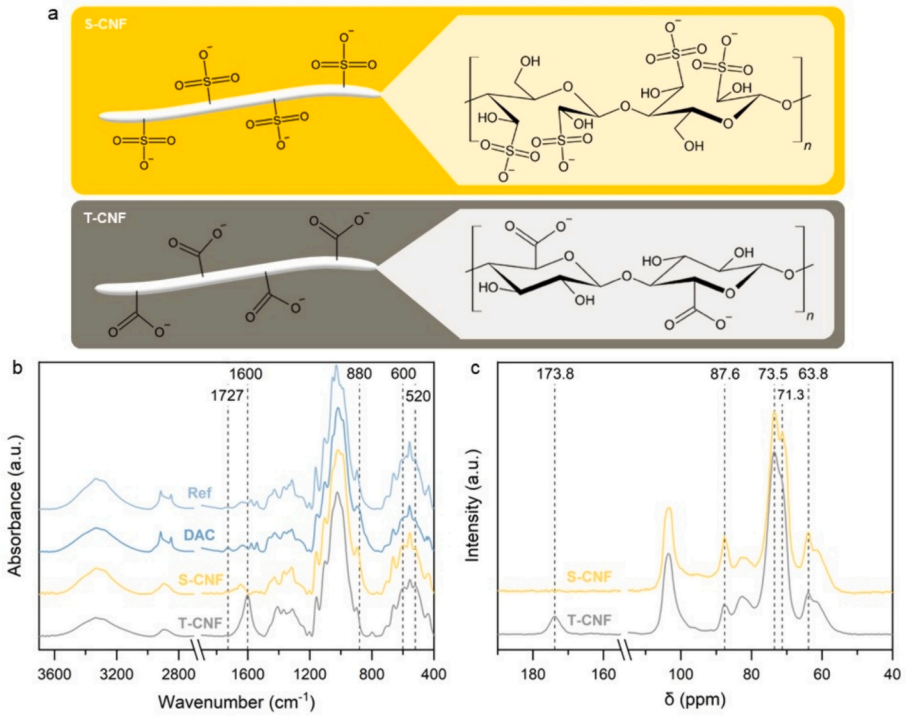

Fig. 1. (a) Surface chemical functionalities and cellulose structures of the sulfonated and TEMPO-oxidized CNF samples, (b) FTIR spectra of reference, intermediate dialdehyde cellulose and the two CNF samples, (c) solid-state 13C CP-MAS NMR spectra of the two CNF samples.

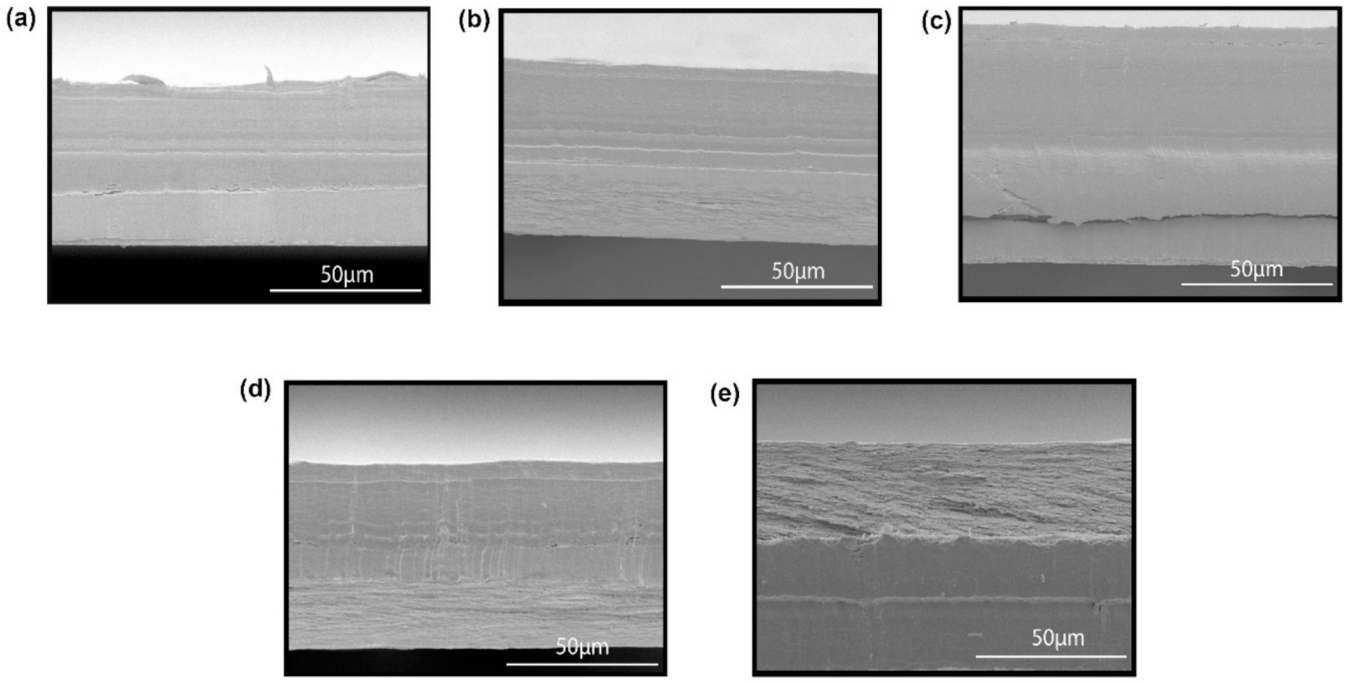

Fig. 2. Cross-sectional SEM images of (a) 100:0, (b) 75:25, (c) 50:50, (d) 25:75, and (e) 0:100 samples.

absence of water in the resulting membranes, caused by oven drying the samples to produce films.

The thermogravimetric curves of modified CNF membranes, obtained in an inert atmosphere, can be found in Fig. 3b for TGA and Fig. S3a for DTG. The S-CNF (0:100) sample has 2 thermal stages and as T-CNF is added, a new stage appears, totaling 3 thermal stages for the rest of the membranes and accelerating their degradation compared to the S-CNF membrane. For all samples, the first stage is related to the evaporation of the residual moisture with a weight loss between 2 and 5 % and the second and third peaks correspond to the sample degradation. As can be seen in both figures, all degradation peaks start and finish at similar temperatures. For instance, the T-CNF membrane (100:0) has temperature ranges from 190 to 264 °C (T_{max} = 233 °C and WL = 12.241 %) and from 270 to 340 °C (T_{max} = 297 °C and WL = 11.982 %) for the second and third stages, respectively. Similar behavior was noticed for 75:25, 50:50, and 25:75 membranes. However, these three

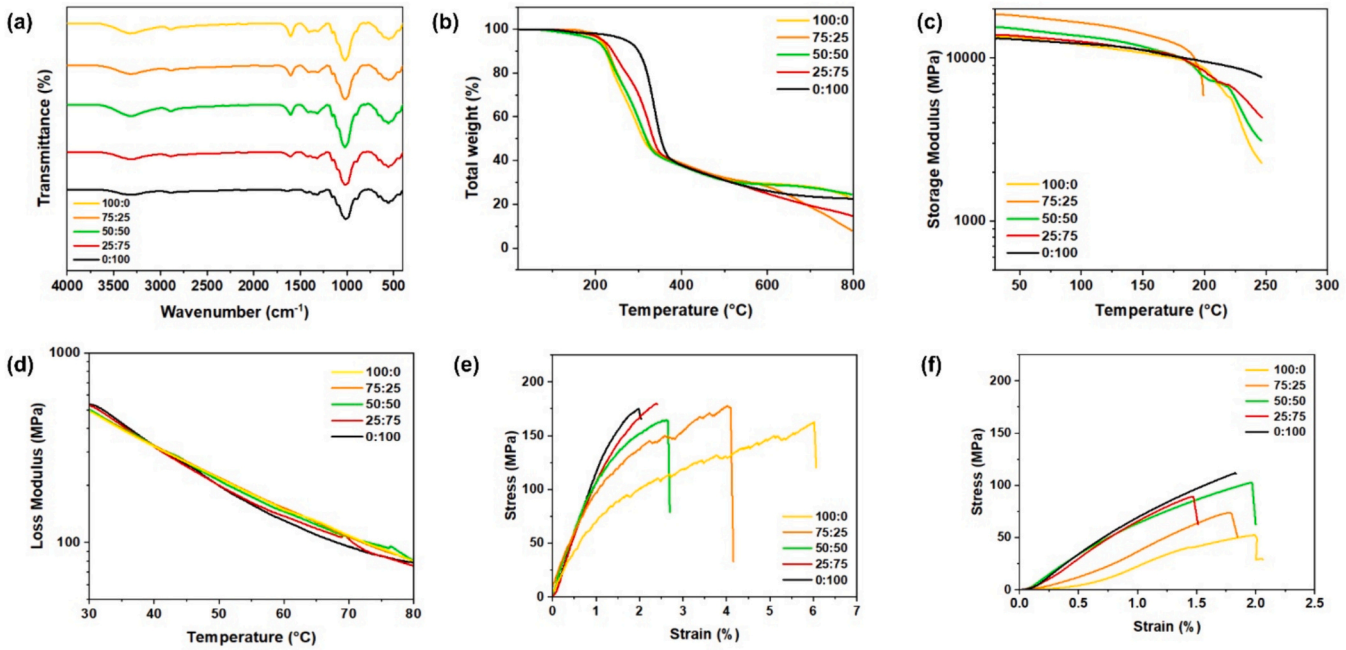

Fig. 3. Mechanical, chemical, and thermal characterization of the modified CNF membranes. (a) FTIR spectra (b) TGA, (c) storage modulus at room RH, (d) storage modulus at 90 % RH(e) Stress-strain curve at 25 °C, and (f) Stress-strain curve at 80 °C of all modified CNF membranes.

membranes had lower percentage degradation around 200 °C than T-CNF. As mentioned before, the sulfonated CNF film has only 2 thermal stages, where the second peak corresponds to its thermal degradation from 259 to 403 °C (T_{max} = 337 °C and WL = 58.28 %) and highest decomposition of the sample. The rate of thermal decomposition of the films decreases and remains at a similar level up to 800 °C.

DMA analysis was carried out to evaluate the mechanical properties of the pure and bicomponent membranes (Fig. 3c–f, Fig. S3b, and S3c). Through this analysis, it is possible to separate the storage modulus E' and the loss modulus E" regions to study the elastic and viscous responses of the polymeric membranes. According to Fig. 3c, 100:0, 0:100, and 25:75 samples exhibit a similar profile with a small decrease of the storage modulus curve around 200 °C and a drop around 230 °C. The 75:25 sample has a substantial higher storage modulus from 30 to around 170 °C, while 50:50 membrane is in the middle of both groups. At 90 % RH, all samples see a progressive decrease in storage modulus as the temperature increases with a dramatic drop around 70 °C for 25:75 (Fig. 3d). Although all curves exhibit slight differences in terms of their storage modulus values, as sulfonated CNF is added into the membrane composition, the resulting membrane exhibits a higher storage modulus from 30 to around 70 °C. The tensile modulus, tensile strength, and elongation at break were calculated using the data presented in Fig. 3e and 5d and are listed in Table 2. As seen in this table, the tensile modulus increases as the sulfonated CNF percentage increases at 25 and 80 °C, with a small decay for 0:100 and 25:75 samples at 25 and 80 °C, respectively. The 100:0 sample has the highest tensile strength at 25 °C and the lowest at 80 °C, while the other samples show similar values, especially at 25 °C. As the sulfonated CNF content increases, the elongation at break of all samples progressively decreases at 25 °C, while the membranes are more comparable at 80 °C. Analogous results were found in the literature for other CNF films. Henriksson, Berglund, Isaksson, Lindström, and Nishino (2008) produced nanocellulose paper from wood pulp via an enzymatic hydrolysis and yielded similar tensile values to those reported here. The resulting paper had very high toughness, a Young's modulus of 13.2 GPa, and high tensile strength (214 MPa) (Henriksson et al., 2008). Vilela et al. (2020, b) showed that bacterial nanocellulose (BNC) membranes (thickness: 69 μm) present Young's modulus of 15.0GPa, tensile strength of 195 MPa and elongation at break of 1.8 %. Bayer et al. (2021) synthesized sulfonated CNF PEMs by spray-deposition and obtained Young's modulus and tensile strength of

Table 2
Properties of modified CNF membranes compared to Nafion 112.

Analysis	Membrane					
	100:0	75:25	50:50	25:75	0:100	[a]Nafion 112
Water uptake (%) at 25 °C	6334	5026	2694	616	102.34	38
IEC (meq/g)	0.0131	0.0128	0.0118	0.0111	0.0133	0.98
Proton conductivity (mS/cm) at 25 °C, 100 % RH	1.11 ± 0.27	1.23 ± 0.58	1.33 ± 0.17	1.37 ± 0.83	1.76 ± 0.78	23
Oxidative degree (%)	66.2 ± 5.6	82.7 ± 2.5	84.0 ± 1.2	83.0 ± 2.6	87.32 ± 3.1	95.3
Hydration number	267,788	217,238	126,814	30,681	4258	8
Storage Modulus (GPa) at 25 °C	13.45 ± 0.21	18.47 ± 0.71	15.51 ± 0.89	13.89 ± 0.65	13.176 ± 0.24	< 220*
Storage Modulus (GPa) at 80 °C	12.56 ± 0.67	17.10 ± 0.34	14.16 ± 0.42	13.03 ± 0.98	12.52 ± 0.23	–
Tensile Modulus (MPa) at 25 °C	9.26 ± 0.12	10.63 ± 0.18	11.51 ± 0.32	11.62 ± 0.27	10.07 ± 0.34	240.5
Tensile Modulus (MPa) at 80 °C	812 ± 32	2521 ± 45	7410 ± 23	6258 ± 49	7540 ± 51	–
Tensile Strength (MPa) at 25 °C	184 ± 2	166.5 ± 10.5	163 ± 0	163 ± 2	123.5 ± 11.5	27.10
Tensile Strength (MPa) at 80 °C	53 ± 4	74 ± 6	103 ± 3	89 ± 7	112 ± 8	–
Elongation at break (%) at 25 °C	5.56 ± 0.56	4.09 ± 0.09	2.75 ± 0.05	2.3 ± 0.08	1.66 ± 0.32	310
Elongation at break (%) at 80 °C	2.06 ± 0.43	1.84 ± 0.63	2.00 ± 0.23	1.51 ± 0.27	1.85 ± 0.78	–

[a] Silva, De Francesco, & Pozio, 2004; Tsen et al., 2011; Jiang et al., 2015; Bayer et al., 2021.

1.09GPa and 42.2 MPa, respectively.

According to Table 2, all membranes have higher storage values than the commercial membranes analyzed in this paper (240.5 MPa for Nafion 112). It is important to highlight that the usual operating temperature range of Nafion is from 20 °C to 80 °C, where 80 °C corresponds to the maximum and more efficient temperature for the membrane, as above this value, the conductivity decreases substantially due to water evaporation. Thus, the mechanical and thermal stability of any PEM should be verified at these temperatures, as these parameters play an important role in the proton conductivity and stability of a film. Based on the TGA and DMA results, these membranes showed potential application due to their mechanical and thermal stability at this temperature range.

3.2.3. *Water interaction, conductivity, and oxidative behavior*

Fig. 4a–c shows the water uptake, IEC, proton conductivity, and hydration number for all modified CNF membrane.

As observed in Fig. 4a, the T-CNF membrane has the highest water uptake (WU) at 25 °C, 40 °C, 60 °C, and 80 °C especially when compared with commercial membranes (38 % for Nafion 112, Table 2). As its concentration decreases the water uptake conversely decreases. Both SO_3^- (sulfonate) and COO^- (carboxylate) groups contribute to the hydrophilicity of the membranes. However, the number of hydrogen bonds present with COO^- is higher than with SO_3^-, causing samples with T-CNF to retain more water molecules into their structure, and consequently have a higher WU.

Although the charge density was measured for the T-CNF (2.39 mmol/g) and S-CNF (0.47 mmol/g) suspensions, the number of active groups in the final membrane are also proportional to this parameter. Consequently, T-CNF exhibits a higher charge density in its suspension, leading to an increased presence of COO- groups in the membrane. This results in higher water uptake, as it correlates with the degree of COO-.

As the temperature increases, the WU of all modified CNF films substantially increases due to high temperatures causing the expansion of the polymer chain and the membrane network. This expansion effect increases the interaction between water and the hydrophilic molecules in the polymer structure, resulting in a higher WU at 80 °C than at 25 °C.

However, it was observed that the high water uptake of T-CNF compromises its mechanical stability resulting in a very fragile sample that easily disintegrates when manipulated during testing. An opposite behavior was observed for the S-CNF, which maintained its structural integrity during and after tests.

The proton conductivity values of the membranes increase as the S-CNF content increases. The dissociation constant associated with the deprotonation of SO_3^- groups is higher than for COO-. Similarly, for pKa, in this case, the pKa of SO_3^- groups is lower than for COO- (Fig. 4b). Initially, a similar trend was expected for IEC. However, a substantial drop occurred as T-CNF was added to the membrane matrix, followed by an increase in the 0:100 samples (S-CNF) (Fig. 4b). It is most likely that the interactions between the T-CNF and S-CNF fibers decrease the membrane's ability to hold positively charged ions. Moreover, the orientation structure of CNF and CNF length might affect the electrochemical properties of the resulting membranes due to their interference in the formation of channels for cation transport in the PEM.

As shown in Fig. 4c, the hydration number of the samples follows the same trend as WU. Although this property is a ratio between WU and IEC, the WU values are much higher than IEC, determining the final result. It is also possible to conclude through this analysis that the number of water molecules surrounding each COO^- is higher than for SO_3^-, resulting in a greater hydration number for samples with the highest content of T-CNF.

The chemical stability of both membranes was investigated with Fenton's reagent for one hour at 80 °C. The T-CNF membrane has a lower oxidative stability, retaining only 66.2 % of its mass, while the other samples maintained over 80 % of their mass after the test (Table 2). Although the IEC and proton conductivity results are similar, we can still observe an increase in those values as the S-CNF percentage increases. A possible reason for this slight effect can be associated with the nature of COO^- and SO_3^-. The charge density of the T-CNF suspension (2.39 mmol/g) surpasses that of the S-CNF suspension (0.47 mmol/g). This difference directly influences the proton conductivity of the bio-based membranes, where a higher percentage of T-CNF correlates with increased proton conductivity. However, the COO^- and SO_3^- groups exhibit distinct acidic natures, leading to an unexpected trend. In this context, the enhanced conductivity in membranes with a greater percentage of S-CNF is attributed to the stronger acidic nature of sulfonic acid groups in S-CNF compared to T-CNF (Guccini et al., 2019; Lander et al., 2022). The membranes with T-CNF also exhibit higher water uptake compared to S-CNF proton exchange membrane (PEM), implying heightened proton conductivity. However, during the water absorption process, the expansion of CNF fibers reduces confined water channels in the membrane, resulting in lower conductivity for T-CNF-based membranes. The high conductivity shown in Table 2 for Nafion 112 is ascribed to the large amount and the high acidity of the sulfonic groups as well as the presence of confined channels between its hydrophobic and hydrophilic domains. Herein, the difference between CNF and Nafion is likely due to the use of functional groups that are significantly less acidic (Guccini et al., 2019). Additionally, a non-negligible fraction of the sulfonate groups was possibly lost during the processing steps, most likely during the vacuum filtration where highly charged polymer chains on the fibril surfaces may have dissolved and been able to escape through the pores of the PVDF membrane and small fractions in the CNF storage and membrane drying.

As mentioned before, the WU is directly proportional to the degree of conductive groups available in the membrane. However, the WU is not directly proportional to the IEC since there exists a background WU in the cellulose fibril network due to nonionic interactions of cellulose-water interactions and network formation (Lander et al., 2022).

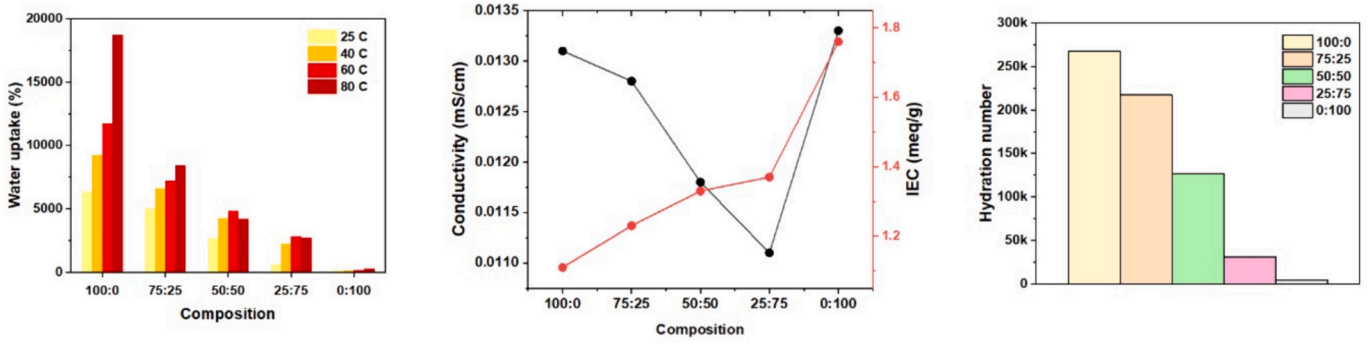

Fig. 4. (a) Water uptake at 25 °C, 40 °C, 60 °C, and 80 °C, (b) Comparison of the IEC and proton conductivity at different CNF composition, and (c) hydration number for all modified CNF membrane.

3.2.4. Transport mechanism

The modification of CNF aimed to improve the electrochemical properties of the resulting biobased PEMs by adding SO_3^- and COO^- groups. These ionic and hydrophilic groups are attached to the linear chain of cellulose (formed by many β(1 → 4) linked D-glucose units) and connected with each other to form hydrophilic domains after hydration. Throughout these groups, the membrane nanostructure enables ionic conduction with the free movement of hydrogen ions in the region where sufficient water is supplied (Fig. 1a). The role of modified cellulose nanofibers is in the formation of channels within the membrane structure Fig. 5a–c *show the mechanism of transport for the T-CNF (100:0), mixed of T-CNF and S-CNF (representing 75:25, 50:50, and 25:75 compositions), and S-CNF membranes, where in any of these membranes the proton transference occurs by the same process. Essentially,* the percolated network of modified CNF present in the PEM structure mimics the interconnected network of hydrophilic sulfonate groups present in Nafion. These ionic channels play a critical role in enhancing the seamless transport of protons, thereby significantly improving the overall operational efficiency of fuel cells.

3.2.5. Feasibility of the bicomponent CNF membranes for a PEM

As previously highlighted, the modification of nanocellulose was needed to add ionic groups into its structure and improve its electrochemical properties for FC application. Even after CNF modification to obtain T-CNF and S-CNF, the IEC and proton conductivity for all membranes (neat and biocomponent) were not comparable to Nafion values. Although important, electrochemical activity is not the only evaluated parameter in a PEM. This membrane should also have excellent mechanical, thermal, and chemical stability before and after application. Based on the results showed previously, all modified CNF membranes have higher or comparable results to Nafion (Table 2), but we could not identify an altogether superior membrane composition between the single and bicomponent films since each analysis showed a different and better performance. For instance, the 75:25 sample had the highest storage modulus at 25 °C while 0:100 film had the highest onset of thermal degradation.

The modified CNFs developed in the present study displays characteristic values that are comparable to some biobased ion-exchange membranes reported in literature, as outlined in Table 3. Examples include membranes composed of CNCs, chitosan, and poly(vinyl alcohol), which exhibit the highest conductivity of 0.642 mS/cm (at 25 °C, fully hydrated) (Gaur et al., 2017). Additionally, the BNC/fucoidan membrane demonstrates a maximum conductivity of 1.6 mS/cm (at 94 °C, with 98 % relative humidity), as obtained by Vilela et al., 2019.

The hypothesis raised in this research is that the combination of T-CNF and S-CNF could beneficially alter the conductivity of the membrane, by providing more charge sites and channels for H^+ ion transport. Many properties can affect the contribution of T-CNF and S-CNF in the electrochemical properties of the final membrane, including the size of the conductive groups (COO^- and SO_3^-), the charge density of the T-CNF and S-CNF suspensions, the acidic nature of COO^- and SO_3^- and the layer organization of the fibers, considering the repulsion between COO^- and SO_3^-. The latter can be directly correlated with the formation of either larger or smaller channels. Although the electrochemical properties of all modified CNF films are significantly lower than those of the Nafion 112 membrane, the findings presented in this research introduce a biobased material with significant thermal, mechanical, and chemical stability (Table 2 and Fig. 3), along with a superhydrophilic capacity that enables a PEM to absorb water while its conductivity progressively

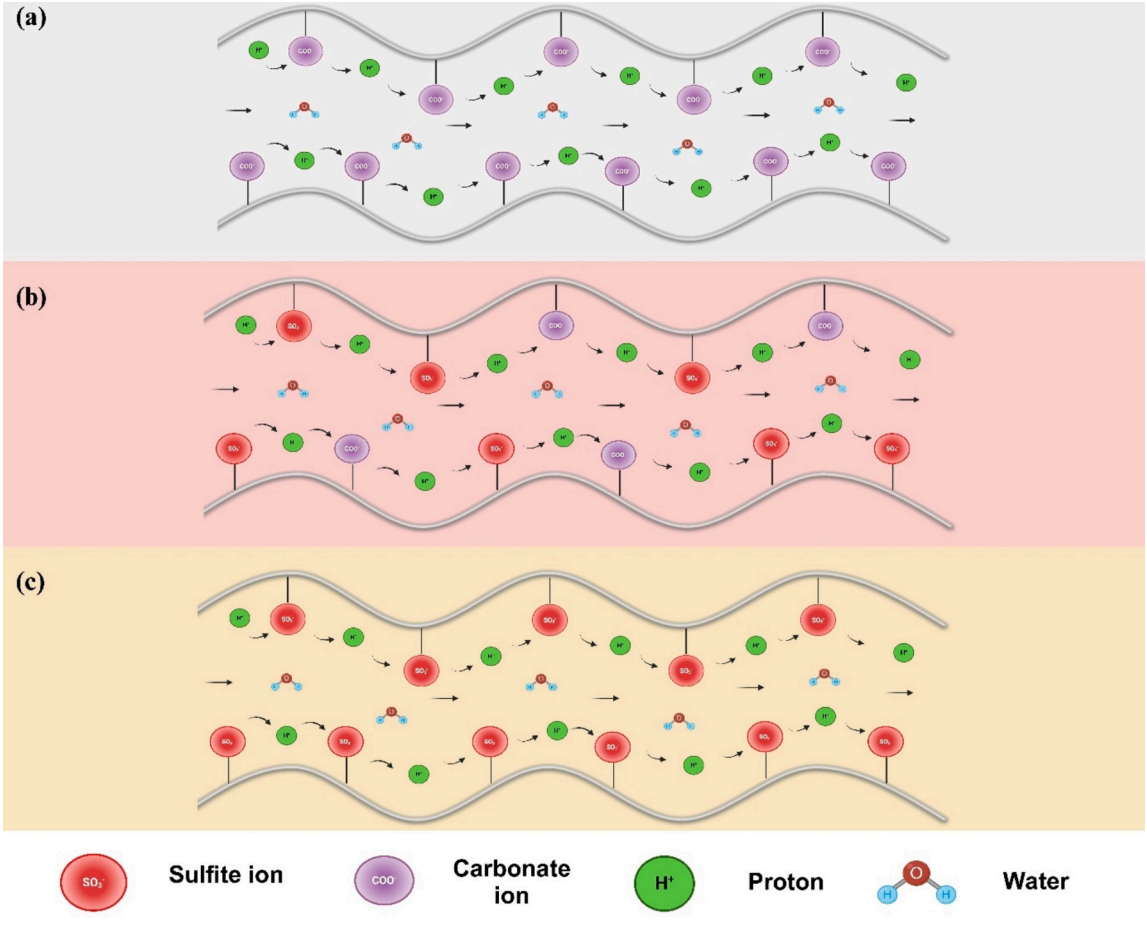

Fig. 5. Graphical representation and transport phenomena of (a) of T-CNF (b) composite of T-CNF and S-CNF, and (c) S-CNF membranes.

Table 3
Examples of partially and fully biobased ion-exchange membranes reported in literature and compared with the present study.

System	Cellulosic substrate	Polyelectrolyte or ionomer	General features	Performance	Ref. #
Fully biobased	Modified CNFs	–	Thickness: (46.2–50) μm IEC_{max}: 0.013 Young's modulus: 13 GPa	σ_{max}: 1.75 mS/cm (at 25 °C and 100 % RH)	This work
	CNC	–	Thickness: 30 μm H_2 permeability: 0.01 barrer	σ_{max}: 4.6 mS/cm (at 120 °C and 100 % RH) OCV: 0.87 V	Bayer et al., 2016
	BNC/LS	–	Thickness: 75 Young's modulus: 8.2 ± 1.6 GPa	23 mS/cm (94 °C, 98 % RH, IP)	Vilela et al., 2020, b
	BNC/Fucoidan	–	Thickness: 79 Young's modulus: 527 MPa	1.6 mS/cm (94 °C, 98 % RH, TP)	Vilela et al., 2019
	Chondroitin sulfate/ citric acid	–	–	37 mS/cm (25 °C, 98 % RH, TP)	Santos et al., 2020
Partially biobased	CNCs	Imidazole	Thickness: 100 μm	σ_{max}: 27 mS/cm (at 140 °C)	Tritt-Goc, Jankowska, Pogorzelec-Glaser, Pankiewicz, & Ławniczak, 2018
	CNCs	CH (46.5 wt%)	Water uptake: 78 %	σ_{max}: 0.642 mS/cm (at RT, 100 % RH, IP)	Gaur et al., 2017
	CNCs	SPAEK (95 wt%, with 10 % COOH groups)	Young's modulus: 526 MPa Water uptake: 77 % (at 80 °C) IEC: 2.49 meq. g^{-1}	σ_{max}: 0.642 mS/cm (at 90 °C RT, 100 % RH, IP)	Ni et al., 2016
	CNCs	SPEEK (96 wt–)	Thickness: 70–80 μm Young's modulus: 3.4 GPa Water uptake: 78.2 % (at 95 °C) IEC: 1.77 meq. g^{-1}	σ_{max}: 186 mS/cm (at 95 °C and 95 % RH)	Bano, Negi, Illathvalappil, Kurungot, & Ramya, 2019
	CNFs	SPES (95 wt%)	Tensile strength: 40 MPa Water uptake: 40 % (at 80 °C)	σ_{max}: 0.05 mS/cm(at 80 °C and 100 % RH)	Xu et al., 2018
	CNFs	Phosphoric acid (0.25 mol dm^{-3}) SPES (95 wt%)	Thickness: 85–120 μm Tensile strength: 28 MPa Water uptake: 43 % (at 80 °C)	σ_{max}: 154 mS/cm (at 80 °C and 100 % RH)	Cai et al., 2018
	CNF	s-PBI (96 wt%)	Thickness: 45–55 μm Young's modulus: 27 GPa Water uptake: 26 % (at 80 °C)	σ_{max}: 66.6 mS/cm (at 140 °C)	Esmaielzadeh & Ahmadizadegan, 2018
	CNF	PAA (97 wt%)	Thickness: 400 μm Tensile stress: 1.85 MPa Swelling ration: 200 %	σ_{max}: 270 mS/cm	Li et al., 2018

BCN: Bacterial nanocellulose; LS: Lignosulfonate; RT: Room temperature; RH: Relative humidity; IP: in-plane configurations; TP: through-plane; CH: Chitosan; SPAEK: sulfonated poly(arylene ether ketone)s; SPEEK: sulfonated poly(ether ether ketone); SPES: sulfonated poly(ether sulfone); s-PBI: sulfonated polybenzimidazole; PAA: poly(acrylic acid); σ: conductivity. Table adapted from Vilela et al., 2019.

increases. Therefore, combining these modified CNFs with other polymers may allow for synthesis of partially bio-based IEMs, reducing the final cost of a commercial PEM, increasing sustainability, and furthering valorizing this biopolymer via a novel application in the growing domain of sustainable energy production and storage (Table 3). The cost analysis for this membrane is out of the scope of this paper. However, *a rough cost analysis considering the reagent prices, the reaction yield, the energy expenses, and the processing time can be made and as expected, the final price was around $77–90/m^2.*

The various measurements of mechanical, thermal, chemical, and electrochemical properties presented in Table 2 demonstrate that tailoring the chemical structure of nanocellulose fibers allows for their integration into a PEM composition, thereby adding value to the product without compromising membrane strength or stability. Consequently, both S-CNF and T-CNF are well-suited as ionomer membranes in real-world PEMFCs. As a potential area for future research, we emphasize the importance of incorporating these materials into an artificial polymer matrix to address existing gaps. This consideration takes into account the thermal, mechanical, and chemical stability of CNF, as well as its high hydrophilic properties that can be utilized to enhance water absorption and, consequently, improve ion conductivity.

4. Conclusion

CNF membranes were prepared and characterized for their integration into a PEMFC configuration. All bio-based PEMs exhibited an impressive thermal stability up to 190 °C and high mechanical properties with a maximum Young's modulus of around 1.15GPa, tensile strength of 0.18GPa, and storage modulus over 13GPa, as well as a high hydrophilicity with a water uptake as high as 6334 %. These results are comparable to bio-based membranes mentioned in the literature and to commercially available membranes. *Based on the results reported and discussed herein, we could not identify an altogether superior membrane composition between the single and bicomponent films since each analysis demonstrated the varying strengths and weakness of each membrane's performance. Moreover, the combination of COO^- and $SO3^-$ groups was not meaningfully effective in altering the membrane's conductivity by enhancing the transport of H^+ ions, as initially hypothesized.* However, the findings presented in this research introduce a bio-based material that could potentially be combined with other polymer matrices, presenting an opportunity to synthesize partial or fully bio-based IEMs. Utilizing modified CNFs as a bio-based template for a commercial PEM would reduce costs, improve sustainability, and valorize cellulose through a new, high value application. The intrinsic renewability and tunability of cellulose-derived materials makes them promising candidates to meet the demands of novel sustainable energy solutions, and these bio-based membranes hold the potential for further enhancement through optimizing support structure materials, blend compositions, and production techniques.

CRediT authorship contribution statement

Fernanda Brito dos Santos: Writing – review & editing, Writing – original draft, Visualization, Methodology, Investigation, Formal analysis, Data curation, Conceptualization. **Joice Kaschuk:** Writing – review & editing, Investigation, Conceptualization. **Gabriel Banvillet:** Writing – review & editing, Investigation, Formal analysis. **Adel Jalaee:** Writing – review & editing, Investigation. **Orlando J. Rojas:** Writing – review & editing, Formal analysis. **E. Johan Foster:** Writing – review & editing, Supervision, Project administration, Funding acquisition, Conceptualization.

Declaration of competing interest

The authors declare that they have no known competing financial interests or personal relationships that could have appeared to influence

the work reported in this paper.

Data availability

Data will be made available on request.

Acknowledgments

The authors gratefully acknowledge the financial support provided by the NSERC Canfor Industrial Research Chair in Advanced Bio-products (# 553449 - 19), NSERC Discovery Grant (RGPIN-2021-03172), the Canada Excellence Research Chair Program (CERC-2018-00006), Canada Foundation for Innovation (Project numbers 022176 and 38623), Pacific Economic Development Canada (PacifiCan), and the British Columbia Ministry of Forest. UBC Centre for High-Throughput Phenogenomics is acknowledged for providing SEM imaging facilities. JK and OJR acknowledge academy of Finland's Flagship Programme under Projects No. 318890 and 318891 (Competence Center for Materials Bioeconomy, FinnCERES.

Appendix A. Supplementary data

Supplementary data to this article can be found online at https://doi.org/10.1016/j.carbpol.2024.122299.

References

Abaspour, A., Tadrisi Parsa, N., & Sadeghi, M. (2014). A new feedback linearization-NSGA-II based control design for PEM fuel cell. *International Journal of Computer Applications, 97*(10), 25–32. https://doi.org/10.5120/17044-7354

Badwal, S. P. S., Giddey, S. S., Munnings, C., Bhatt, A. I., & Hollenkamp, A. F. (2014). Emerging electrochemical energy conversion and storage technologies. *Frontiers in Chemistry, 2*. https://doi.org/10.3389/fchem.2014.00079

Bano, S., Negi, Y. S., Illathvalappil, R., Kurungot, S., & Ramya, K. (2019). Studies on nano composites of SPEEK/ethylene glycol/cellulose nanocrystals as promising proton exchange membranes. *Electrochimica Acta, 293*, 260–272. https://doi.org/10.1016/j.electacta.2018.10.029

Banvillet, G., Depres, G., Belgacem, N., & Bras, J. (2021). Alkaline treatment combined with enzymatic hydrolysis for efficient cellulose nanofibrils production. *Carbohydrate Polymers, 255*, Article 117383. https://doi.org/10.1016/j.carbpol.2020.117383

Bayer, T., Cunning, B. V., Selyanchyn, R., Nishihara, M., Fujikawa, S., Sasaki, K., & Lyth, S. M. (2016). High temperature proton conduction in nanocellulose membranes: Paper fuel cells. *Chemistry of Materials, 28*(13), 4805–4814. https://doi.org/10.1021/acs.chemmater.6b01990

Bayer, T., Cunning, B. V., Šmíd, B., Selyanchyn, R., Fujikawa, S., Sasaki, K., & Lyth, S. M. (2021). Spray deposition of sulfonated cellulose nanofibers as electrolyte membranes in fuel cells. *Cellulose, 28*(3), 1355–1367. https://doi.org/10.1007/s10570-020-03593-w

Benhamou, K., Dufresne, A., Magnin, A., Mortha, G., & Kaddami, H. (2014). Control of size and viscoelastic properties of nanofibrillated cellulose from palm tree by varying the TEMPO-mediated oxidation time. *Carbohydrate Polymers, 99*, 74–83. https://doi.org/10.1016/j.carbpol.2013.08.032

Cai, Z., Li, R., Xu, X., Sun, G., Zhuang, X., Liu, Y., & Cheng, B. (2018). Embedding phosphoric acid-doped cellulose nanofibers into sulfonated poly (ether sulfone) for proton exchange membrane. *Polymer, 156*, 179–185. https://doi.org/10.1016/j.polymer.2018.10.013

Baker, R., & Zhang, J. (2011). Proton exchange membrane or polymer electrolyte membrane (PEM) fuel cells. The Electrochemical Society. https://knowledge.electrochem.org/encycl/art-f04-fuel-cells-pem.htm#dtop.

D20 Committee. (n.d.). Test method for water absorption of plastics. ASTM International. doi:https://doi.org/10.1520/D0570-22.

Di Virgilio, M., Basso Peressut, A., Arosio, V., Arrigoni, A., Latorrata, S., & Dotelli, G. (2023). Functional and environmental performances of novel electrolytic membranes for PEM fuel cells: A lab-scale case study. *Clean Technologies, 5*(1), 74–93. https://doi.org/10.3390/cleantechnol5010005

Esmaielzadeh, S., & Ahmadizadegan, H. (2018). Construction of proton exchange membranes under ultrasonic irradiation based on novel fluorine functionalizing sulfonated polybenzimidazole/cellulose/silica bionanocomposite. *Ultrasonics Sonochemistry, 41*, 641–650. https://doi.org/10.1016/j.ultsonch.2017.10.029

Feng, M., Qu, R., Wei, Z., Wang, L., Sun, P., & Wang, Z. (2015). Characterization of the thermolysis products of Nafion membrane: A potential source of perfluorinated compounds in the environment. *Scientific Reports, 5*(1), 9859. https://doi.org/10.1038/srep09859

Gadim, T. D. O., Figueiredo, A. G. P. R., Rosero-Navarro, N. C., Vilela, C., Gamelas, J. A. F., Barros-Timmons, A., … Figueiredo, F. M. L. (2014). Nanostructured bacterial cellulose–poly(4-styrene sulfonic acid) composite membranes with high storage modulus and protonic conductivity. *ACS Applied Materials & Interfaces, 6*(10), 7864–7875. https://doi.org/10.1021/am501191t

García, Á., Torrero, J., Retuerto, M., & Rojas, S. (2022). Metal-containing heteroatom doped carbon nanomaterials for ORR, OER, and HER. In *Nanomaterials for Electrocatalysis* (pp. 169–211). Elsevier. https://doi.org/10.1016/B978-0-323-85710-9.00012-5.

Gaur, S. S., Dhar, P., Sonowal, A., Sharma, A., Kumar, A., & Katiyar, V. (2017). Thermo-mechanically stable sustainable polymer based solid electrolyte membranes for direct methanol fuel cell applications. *Journal of Membrane Science, 526*, 348–354. https://doi.org/10.1016/j.memsci.2016.12.030

Guccini, V., Carlson, A., Yu, S., Lindbergh, G., Lindström, R. W., & Salazar-Alvarez, G. (2019). Highly proton conductive membranes based on carboxylated cellulose nanofibres and their performance in proton exchange membrane fuel cells. *Journal of Materials Chemistry A, 7*(43), 25032–25039. https://doi.org/10.1039/C9TA04898G

Henriksson, M., Berglund, L. A., Isaksson, P., Lindström, T., & Nishino, T. (2008). Cellulose nanopaper structures of high toughness. *Biomacromolecules, 9*(6), 1579–1585. https://doi.org/10.1021/bm800038n

Hou, X., Liu, Z., Wei, Y., Zhao, Q., Dong, J., Liu, B., Sun, Z., Shi, T., Zhang, M., & Hu, W. (2017). Proton conducting nanocomposite membranes of nanocellulose reinforced poly(arylene ether ketone)s containing sulfonic/carboxylic groups. *Solid State Ionics, 311*, 31–40. https://doi.org/10.1016/j.ssi.2017.08.019

Irannejad, N., & Rezaei, B. (2022). Three-dimensional electrodes. In *Electrochemical sensors* (pp. 177–212). Elsevier. https://doi.org/10.1016/B978-0-12-823148-7.00007-6.

Jalaee, A., Kamkar, M., French, V., Rojas, O. J., & Foster, E. J. (2023). Direct milling: Efficient, facile, and green method for processing fibrillated cellulose/polymeric nanocomposites with boosted thermomechanical and rheological performance. *Carbohydrate Polymers, 314*. https://doi.org/10.1016/j.carbpol.2023.120932

Jiang, G., Zhang, J., Qiao, J., Jiang, Y., Zarrin, H., Chen, Z., & Hong, F. (2015). Bacterial nanocellulose/Nafion composite membranes for low temperature polymer electrolyte fuel cells. *Journal of Power Sources, 273*, 697–706. https://doi.org/10.1016/j.jpowsour.2014.09.145

Kim, J., & Yang, M. (2023). Chapter 18 - Hydrogen production methods: Benefits, opportunities, costs, and risks. *Hydrogen Economy.*, 573–594. https://doi.org/10.1016/B978-0-323-99514-6.00018-2

Kubicki, J. D., Yang, H., Sawada, D., O'Neill, H., Oehme, D., & Cosgrove, D. (2018). The shape of native plant cellulose microfibrils. *Scientific Reports, 8*(1), 13983. https://doi.org/10.1038/s41598-018-32211-w

Lander, S., Erlandsson, J., Vagin, M., Gueskine, V., Korhonen, L., Berggren, M., … Crispin, X. (2022). Sulfonated cellulose membranes: Physicochemical properties and ionic transport versus degree of Sulfonation. *Advanced Sustainable Systems, 6*(11), Article 2200275. https://doi.org/10.1002/adsu.202200275

Larsson, P. A., Kochumalayil, J., & Wågberg, L. (2013). *Oxygen and water vapour barrier films with low moisture sensitivity fabricated from self-crosslinking fibrillated cellulose* (pp. 851–866). https://doi.org/10.15376/frc.2013.2.851

Li, L., Liu, L., Qing, Y., Zhang, Z., Yan, N., Wu, Y., & Tian, C. (2018). Stretchable alkaline poly(acrylic acid) electrolyte with high ionic conductivity enhanced by cellulose nanofibrils. *Electrochimica Acta, 270*, 302–309. https://doi.org/10.1016/j.electacta.2018.03.088

Liimatainen, H., Visanko, M., Sirviö, J., Hormi, O., & Niinimäki, J. (2013). Sulfonated cellulose nanofibrils obtained from wood pulp through regioselective oxidative bisulfite pre-treatment. *Cellulose, 20*(2), 741–749. https://doi.org/10.1007/s10570-013-9865-y

Mattos, B. D., Tardy, B. L., & Rojas, O. J. (2019). Accounting for substrate interactions in the measurement of the dimensions of cellulose nanofibrils. *Biomacromolecules, 20*(7), 2657–2665. https://doi.org/10.1021/acs.biomac.9b00432

Ni, C., Wei, Y., Hu, Q., Li, X., Liu, B., Zhao, Q., Zhang, M., Li, Y., & Hu, W. (2016). Nanocystalline cellulose reinforced sulfonated fluorenyl-containing polyaryletherketones for proton exchange membranes. *Solid State Ionics, 297*, 29–35. https://doi.org/10.1016/j.ssi.2016.09.027

Painter, T. J. (1988). Control of depolymerisation during the preparation of reduced dialdehyde cellulose. *Carbohydrate Research, 179*, 259–268. https://doi.org/10.1016/0008-6215(88)84123-5

Peighambardoust, S. J., Rowshanzamir, S., & Amjadi, M. (2010). Review of the proton exchange membranes for fuel cell applications. *International Journal of Hydrogen Energy, 35*(17), 9349–9384. https://doi.org/10.1016/j.ijhydene.2010.05.017

Plappert, S. F., Quraishi, S., Pircher, N., Mikkonen, K. S., Veigel, S., Klinger, K. M., … Liebner, F. W. (2018). Transparent, flexible, and strong 2,3-dialdehyde cellulose films with high oxygen barrier properties. *Biomacromolecules, 19*(7), 2969–2978. https://doi.org/10.1021/acs.biomac.8b00536

Saito, T., Kimura, S., Nishiyama, Y., & Isogai, A. (2007). Cellulose nanofibers prepared by TEMPO-mediated oxidation of native cellulose. *Biomacromolecules, 8*(8), 2485–2491. https://doi.org/10.1021/bm0703970

Santos, F. M., Barbosa, P. C., Pereira, R. F. P., Silva, M. M., Gonçalves, H. M. R., Nunes, S. C., … De Zea Bermudez, V. (2020). Proton conducting electrolytes composed of chondroitin sulfate polysaccharide and citric acid. *European Polymer Journal, 124*, Article 109453. https://doi.org/10.1016/j.eurpolymj.2019.109453

Sharma, P. P., & Kim, D. (2022). A facile and sustainable enhancement of anti-oxidation stability of nafion membrane. *Membranes, 12*(5), 521. https://doi.org/10.3390/membranes12050521

Silva, R. F., De Francesco, M., & Pozio, A. (2004). Tangential and normal conductivities of Nafion® membranes used in polymer electrolyte fuel cells. *Journal of Power Sources, 134*(1), 18–26. https://doi.org/10.1016/j.jpowsour.2004.03.028

Spence, K. L., Venditti, R. A., Rojas, O. J., Habibi, Y., & Pawlak, J. J. (2011). A coMParative study of energy consumption and physical properties of

microfibrillated cellulose produced by different processing methods. *Cellulose, 18*(4), 1097–1111. https://doi.org/10.1007/s10570-011-9533-z

Taheri, H., & Samyn, P. (2016). Effect of homogenization (microfluidization) process parameters in mechanical production of micro- and nanofibrillated cellulose on its rheological and morphological properties. *Cellulose, 23*(2), 1221–1238. https://doi.org/10.1007/s10570-016-0866-5

Thomas, L. H., Forsyth, V. T., Šturcová, A., Kennedy, C. J., May, R. P., Altaner, C. M., … Jarvis, M. C. (2012). Structure of cellulose microfibrils in primary cell walls from collenchyma. *Plant Physiology, 161*(1), 465–476. https://doi.org/10.1104/pp.112.206359

Tritt-Goc, J., Jankowska, I., Pogorzelec-Glaser, K., Pankiewicz, R., & Ławniczak, P. (2018). Imidazole-doped nanocrystalline cellulose solid proton conductor: Synthesis, thermal properties, and conductivity. *Cellulose, 25*(1), 281–291. https://doi.org/10.1007/s10570-017-1555-8

Tsen, W.-C., Chuang, F.-S., Shu, Y.-C., Chen, C.-C., Gong, C., & Wen, S. (2011). SPPO/PEI-based acid-base blend membranes for direct methanol fuel cells. *E-Polymers, 11*(1). https://doi.org/10.1515/epoly.2011.11.1.770

Vilela, C., Morais, J. D., Silva, A. C. Q., Muñoz-Gil, D., Figueiredo, F. M. L., Silvestre, A. J. D., & Freire, C. S. R. (2020). Flexible nanocellulose/lignosulfonates ion-conducting separators for polymer electrolyte fuel cells. *Nanomaterials, 10*(9), 1713. https://doi.org/10.3390/nano10091713

Vilela, C., Silva, A. C. Q., Domingues, E. M., Gonçalves, G., Martins, M. A., Figueiredo, F. M. L., … Freire, C. S. R. (2020). Conductive polysaccharides-based proton-exchange membranes for fuel cell applications: The case of bacterial cellulose and fucoidan. *Carbohydrate Polymers, 230*, Article 115604. https://doi.org/10.1016/j.carbpol.2019.115604

Vilela, C., Silvestre, A. J. D., Figueiredo, F. M. L., & Freire, C. S. R. (2019). Nanocellulose-based materials as components of polymer electrolyte fuel cells. *Journal of Materials Chemistry A, 7*(35), 20045–20074. https://doi.org/10.1039/C9TA07466J

Wang, X. X., Swihart, M. T., & Wu, G. (2019). Achievements, challenges and perspectives on cathode catalysts in proton exchange membrane fuel cells for transportation. *Nature Catalysis, 2*(7), 578–589. https://doi.org/10.1038/s41929-019-0304-9

Winter, M., & Brodd, R. J. (2004). What are batteries, fuel cells, and supercapacitors? *Chemical Reviews, 104*(10), 4245–4270. https://doi.org/10.1021/cr020730k

Xu, X., Li, R., Tang, C., Wang, H., Zhuang, X., Liu, Y., Kang, W., & Shi, L. (2018). Cellulose nanofiber-embedded sulfonated poly (ether sulfone) membranes for proton exchange membrane fuel cells. *Carbohydrate Polymers, 184*, 299–306. https://doi.org/10.1016/j.carbpol.2017.12.074

Zhao, G., Xu, X., Di, Y., Wang, H., Cheng, B., Shi, L., Zhu, Y., Zhuang, X., & Yin, Y. (2019). Amino acid clusters supported by cellulose nanofibers for proton exchange membranes. *Journal of Power Sources, 438*, Article 227035. https://doi.org/10.1016/j.jpowsour.2019.227035

Zhu, L.-Y., Li, Y.-C., Liu, J., He, J., Wang, L.-Y., & Lei, J.-D. (2022). Recent developments in high-performance Nafion membranes for hydrogen fuel cells applications. *Petroleum Science, 19*(3), 1371–1381. https://doi.org/10.1016/j.petsci.2021.11.004